Atmos. Meas. Tech. Discuss., doi:10.5194/amt-2017-26, 2017
Manuscript under review for journal Atmos. Meas. Tech.
Discussion started: 15 February 2017

Atmospheric Measurement Techniques Discussions

A variational technique to estimate snowfall rate from coincident radar, snowflake, and fallspeed observations

Steven J. Cooper[1], Norman B. Wood[2], Tristan S. L'Ecuyer[3]

[1]Department of Atmospheric Sciences, University of Utah, Salt Lake City, UT, USA
[2]Cooperative Institute for Meteorological Satellite Studies, University of Wisconsin-Madison, Madison, WI, USA
[3]Department of Atmospheric and Oceanic Sciences, University of Wisconsin-Madison, Madison, WI, USA

Correspondence to: Steven J. Cooper (steve.cooper@utah.edu)

Abstract. Estimates of snowfall rate as derived from radar reflectivities alone are non-unique. Different combinations of snowflake microphysical properties and particle fallspeeds can conspire to produce nearly identical snowfall rates for given radar reflectivity signatures. Such ambiguities can result in retrieval uncertainties on the order of 100-200% for individual events. Here, we use observations of particle size distribution (PSD), fallspeed, and snowflake habit from the Multi-Angle Snow Camera (MASC) to constrain estimates of snowfall derived from Ka-band Zenith Radar (KAZR) measurements at the ARM NSA Barrow Climate Facility site. MASC measurements of microphysical properties with uncertainties are introduced into a modified form of the optimal-estimation CloudSat snowfall algorithm (2C-SNOW-PROFILE) via the a priori guess and variance terms. Use of MASC fallspeed, MASC PSD, and CloudSat snow particle model as base assumptions resulted in retrieved total accumulations with a -18% difference relative to nearby National Weather Service observations over five snow events. Use of different but reasonable combinations of retrieval assumptions resulted in estimated snowfall accumulations with differences ranging from -64% to + 94% for the same storm events. Retrieved snowfall rates were particularly sensitive to assumed fallspeed and habit, suggesting that in-situ measurements can help to constrain key snowfall retrieval uncertainties. More accurate knowledge of these properties dependent upon location and meteorological conditions should help refine and improve ground and space-based radar estimates of snowfall.

1 Introduction

The high-latitude regions play a critical role in shaping climate response to anthropogenic forcing. Model predictions suggest that it is these areas that are most susceptible to change and will experience the most dramatic temperature increase in response to the release of greenhouse gases into the atmosphere (Manabe and Stouffer, 1980; Holland and Bitz, 2003; Serreze and Francis, 2006). Observed changes in the Arctic over the late 20th century and early 21st century have been

Atmos. Meas. Tech. Discuss., doi:10.5194/amt-2017-26, 2017
Manuscript under review for journal Atmos. Meas. Tech.
Discussion started: 15 February 2017

Atmospheric Measurement Techniques Discussions

dramatic and have included increased surface temperature and decreased sea ice, permafrost, glacial ice sheet, and spring arctic snow cover extents (Serreze *et al.*, 2000; Frauenfeld *et al*., 2004; Dyurgerov and Meier, 2005; Stroeve *et al*., 2008, Brown et al., 2010; Stroeve et al., 2014, Perlwitz et al., 2015, among numerous others).

Snowfall can dramatically change surface conditions at high-latitude regions, acting to increase shortwave surface albedo while impacting sensible and latent heat fluxes and longwave emission (Cohen and Rind, 1991). Changes in snow cover can feed back on snow cover, sea ice, and permafrost distributions (Brown, 2000; Ramonovsky, 2002; Holland et al., 2006; Vavrus, 2007), where the effects on permafrost in turn may affect high-latitude carbon storage. Snowfall changes at higher north latitudes may also impact freshening of the North Atlantic Ocean and the strength of the Atlantic Meridional Overturning Circulation. Peterson et al. (2006) attributed more than half of the cumulative freshwater input anomaly in the Arctic and high-latitude North Atlantic Oceans over the previous fifty years to increases in net precipitation over land and oceans, exceeding the estimated contributions from glacial melt and sea ice reduction. Snowfall is also important as it provides mass influx for vast glacial ice sheets such as those found in Antarctica and Greenland (Lenaerts et al., 2013; Palerme et al., 2014). The distribution of snowfall helps define ice sheet dynamics, and the relative difference between snowfall and melt will impact the long-term survival of these glaciers (Van Tricht et al., 2016). Significant loss of ice sheets may have deleterious effects on human society through a corresponding rise of global ocean levels. (Gardner et al., 2013; Jacob et al., 2013)

The quantitative estimation of snowfall at the global scale from spaceborne measurements has occurred only recently. Initial retrieval approaches were based on passive microwave measurements (Skofronick-Jackson et al., 2004; Noh et al. 2006) with a shift in emphasis to radar observations with the launch of the CloudSat Cloud Profiling Radar (CPR) in 2006. Matrosov et al. (2007) and Liu (2008) demonstrated the first-order capability of the CloudSat CPR to retrieve vertical profiles of dry snowfall. Kulie and Bennartz (2009), in turn, used CloudSat CPR reflectivities to estimate global dry snowfall rate for a year of CloudSat data. They found that snowfall estimates depended critically upon assumed relationships between radar reflectivity and snowfall particle size distributions and shapes.

These studies suggest that estimates of snowfall as derived from radar reflectivities alone are non-unique. Numerous different combinations of snowflake microphysical properties and snow particle fallspeeds may yield nearly identical surface snowfall rates for a given reflectivity profile. As such, use of traditional Z-S relationships to quantify snowfall cannot be expected to produce accurate results for all snowfall events.

From an operational retrieval perspective, clever selection of representative snowflake microphysical properties may produce estimates of snowfall amounts that agree well with reported values for climate or regional applications. For example, Wood et al. (2015, but see also Wood, 2011) developed snowflake models for the CloudSat snowfall retrieval algorithm based upon

Atmos. Meas. Tech. Discuss., doi:10.5194/amt-2017-26, 2017
Manuscript under review for journal Atmos. Meas. Tech.
Discussion started: 15 February 2017

Atmospheric Measurement Techniques Discussions

field campaigns focused on cold-season clouds and precipitation, principally the Canadian CloudSat-CALIPSO Validation Project (C3VP, Hudak et al. 2006). They used this a priori knowledge of snowfall microphysics to refine expected snowfall-radar reflectivity relationships for the optimal-estimation (Rodgers, 2000) based CloudSat snowfall retrieval scheme used for the CloudSat 2C-SNOW-PROFILE product. The product provides estimates of snow size distribution and bulk properties (water content and snowfall rate) at the surface and aloft over land, ice and ocean surfaces. These estimates have proven valuable for assessing snowfall budgets in remote regions (Palerme et al. 2014; Kulie et al., 2016), providing data for testing global climate models (Palerme et al., 2016; Christensen et al., 2016), and evaluating the performance of ground-based radar measurements of snowfall (Norin et al., 2015).

Despite such efforts, validation activities suggest that uncertainties in retrieved snowfall rates can still be on the order of 200% for individual snow events (Wood, 2011). In our retrieval scheme, instead of using a priori guesses of snowflake microphysical properties from field campaigns such as C3VP, we used co-incident observations of snowflake microphysical properties from the Multiple-Angle Snow Camera (MASC, Garrett et al., 2012) to constrain the radar-based retrieval approach. The MASC takes multiple images of snowflakes in free fall while simultaneously measuring fallspeed. From these pictures, estimates of snowflake maximum particle dimension, habit, and other properties that could be used to refine a radar retrieval scheme are estimated. It should be noted, however, that any instrument that measures snow particle properties or fallspeed, e.g. the Precipitation Imaging Package (PIP), could replace the role of the MASC in the variational approach presented in this work.

We describe here a retrieval technique for snowfall rate and its application to five snow events as observed at the Atmospheric Radiation Measurement (ARM) North Slope Alaska Climate Facility Site at Barrow. Our scheme uses ground-based Ka-band Zenith Radar (KAZR) measurements for reflectivity profiles and was directly modified from the W-band CloudSat 2C-SNOW-PROFILE algorithm. The flexible optimal-estimation framework was used to incorporate co-incident MASC observations into the radar-based scheme through the retrieval a priori terms. A primary objective was to identify those combinations of retrieval assumptions that allowed the best match with snowfall observations at the Barrow site for five snow events during April and May 2014. Another objective was to quantify the sensitivity of snowfall rate retrieval results to the key microphysical assumptions of particle size distribution, habit, and fallspeed from the MASC. These results were contrasted with snowfall rates found using alternate assumptions such as Locatelli and Hobbs (1974, hereafter LH74) particle dimension- fallspeed parameterizations, observed KAZR Doppler velocities, and previous field campaign estimates of snow particle size distributions. In Section 2, we discuss methodology including the CloudSat snowfall retrieval scheme, the MASC observations, and the combined radar- MASC retrieval approach. In Section 3, we explore the application of the combined scheme to five snowfall events observed at the Barrow site. In section 4, we discuss the implications of our results for the utility of ground-based in-situ measurements to refine and improve radar retrievals of snowfall.

Atmos. Meas. Tech. Discuss., doi:10.5194/amt-2017-26, 2017
Manuscript under review for journal Atmos. Meas. Tech.
Discussion started: 15 February 2017

Atmospheric Measurement Techniques Discussions

2 Methodology

2.1 CloudSat Snowfall Retrieval Scheme

The CloudSat snowfall retrieval algorithm uses profiles of W-band 94 GHz radar reflectivity to estimate vertical profiles of snow properties. The flexible optimal-estimation approach is used to combine measurements and a priori microphysical information into a common retrieval cost function. Specifically, the scheme assumes an exponential form for snow particle size distributions for each radar reflectivity bin as in Eq. (1),

$$N(D)=N_0\exp(-\lambda D), \quad (1)$$

where λ is PSD slope parameter, N_0 is its intercept, and D is particle maximum dimension (Heymsfield et al., 2008). For our implementation, the PSD slope parameter is allowed to vary with height but the number density is held constant given the limited number of independent observations from the radar. (Note that the uniform N_0 used in this work represents a divergence from the current CloudSat algorithm in which number density is allowed to vary with height.) A priori assumptions of particle mass-diameter and diameter- fallspeed relationships for D in Eq. (1) allow the determination of snow water content and snowfall rate for each radar range bin.

For the CloudSat algorithm, the required a priori microphysical and scattering properties were determined from analyses of snow observations from field campaigns focused on cold-season clouds and precipitation, principally the Canadian CloudSat-CALIPSO Validation Project (C3VP, Hudak et al. 2006). Snowflake particle models were constructed based upon observed mass and horizontally-projected area as a function of particle size (Wood et al., 2015). These efforts were somewhat unique in that they explicitly use ground-based observations to refine forward model assumptions for the retrieval, an idea we will return to for our combined radar-MASC scheme as described below. Scattering properties for the snowflake particle models were developed through use of the Discrete Dipole Approximation (DDA, Draine and Flatau, 1994) method. DDA replaces the true particle shape with an approximate shape constructed as a three-dimensional array of small, cubic ice dipoles.

Figure 1 shows the particle models developed for the CloudSat algorithm. These particle models, intended to simulate the coarse features of snow particles, consist of solid-ice dipoles intermixed with empty (i.e., air-occupied) dipole locations to meet observed mass and horizontally-projected area (Ap) constraints. Analyses of disdrometer, X-band radar, 2D video disdrometer and Snow Video Imager observations for four significant C3VP snow events provided best-estimate mass-dimension and Ap-dimension relationships (Wood et al., 2015). Scattering calculations for a range of shapes conforming to these constraints suggested that backscatter cross-sections can vary by two orders of magnitude between these models for a given particle size typical of snowfall.

Atmos. Meas. Tech. Discuss., doi:10.5194/amt-2017-26, 2017
Manuscript under review for journal Atmos. Meas. Tech.
Discussion started: 15 February 2017

Atmospheric Measurement Techniques Discussions

For the C3VP snow events, these particle models were evaluated by testing against coincident, observed W-band radar reflectivities (Wood et al., 2015). DDA scattering properties were used in combination with disdrometer observations of snow particle size distributions (the Snowflake Video Imager, Newman et al., 2009) to calculate synthetic W-band reflectivities. These synthetic reflectivities were then plotted versus observed reflectivities as in Figure 2. Minimization of these differences suggested that the B8pr-30 model best matched observations for the C3VP snow events.

For our study, we will use this B8pr-30 particle model as a base assumption for our Barrow storm events. Given the non-uniqueness of the snowfall retrieval problem, however, it is possible that sources of error other than particle model may have compensated to allow observed and synthetic reflectivities to match as in Figure 2. We will examine the sensitivity of retrieved snowfall rate to MASC observations of shape, particle dimension, and fallspeed to better understand this issue as discussed in Section 2.3 below.

2.2 Multi-Angle Snowflake Camera

The Multi-Angle Snowflake Camera (MASC) takes high-resolution multi-angle photographs of snowflakes as they settle near the surface. It simultaneously measures snowflake fallspeed. The MASC consists of three cameras each pointing at an identical focal point approximately 4 inches away in a ring opening. This ring houses a system of near-infrared emitter-detector pairs, arranged in two arrays that are separated vertically by about 1.25 inches. If a hydrometeor passes through both upper and lower arrays, the MASC will trigger each of the three cameras and flash a bank of lights aimed at the center of the camera depth of field. Fallspeed is calculated from the time it takes to traverse the distance between the upper and lower triggering array.

Given images from the MASC, it is possible to derive estimates of properties such as particle shape, aspect ratio, maximum dimension, complexity, and orientation (Garrett et al., 2012; Garrett and Yuter, 2014; Garrett et al., 2015). Here, specifically, we use observations of maximum dimension and habit to constrain uncertainties inherent to radar-based retrievals of snow rate. For example, Figure 3 shows typical snowflakes observed at the NSA Barrow Climate Facility Site during the Spring 2014 MASC deployment. Observed habits include graupel, columns, plates, and aggregate combinations of each. Such observations of shape can be used to select the most appropriate particle model for a given precipitation scene or to identify those scenes in which none of the currently available particle models will be expected to produce a good fit.

Atmos. Meas. Tech. Discuss., doi:10.5194/amt-2017-26, 2017
Manuscript under review for journal Atmos. Meas. Tech.
Discussion started: 15 February 2017

Atmospheric Measurement Techniques Discussions

Observations of fallspeed from the MASC, in turn, can be used to translate retrieved cloud snow water content to a snowfall rate. In this work, we contrast retrieved snowfall rates found using MASC observations, near-surface Doppler measurements, and LH74 particle dimension- fallspeed relationships.

2.3 Combined Radar- MASC Retrieval

The MASC deployment to the ARM NSA Barrow Climate Facility Site in Spring 2014 provided an ideal opportunity to employ our combined radar-MASC snowfall retrieval scheme. Given lack of W-band radar measurements during this time period, we use Ka-band Zenith radar (KAZR) observations for this study. In this section, we present sample observations from a Barrow snowstorm to illustrate how we merge MASC information into our radar-based retrieval scheme. We focus specifically on MASC observations of particle maximum dimension, particle model, and fallspeed.

Figure 4 shows KAZR reflectivities for an all-day April 23 snow event at Barrow. The MASC images shown below the reflectivity plot indicate typical observed snowflakes selected as a function of time. For example, these images suggest rimed graupel-like particles around 4 UTC when the KAZR reflectivities suggest the most cloud vertical development. The snowflakes transitioned to sector plate type crystals and aggregates as the cloud tops lowered and became more homogenous.

To understand precisely how we incorporate desired MASC information into the modified KAZR snowfall scheme, it is useful to consider the optimal-estimation approach used in the CloudSat retrieval scheme. Letting **x** denote the vector of snowfall properties to be retrieved, the optimal estimation technique consists of minimizing a combination of the variance between the set of observations, **y**, and a corresponding set of simulated measurements, F(**x**), and between **x** and a suitable a priori guess, **a**. Assuming Gaussian statistics, this is accomplished by minimizing the scalar cost function,

$$\Phi(x,y,a) = (y - F(x))^T S_y^{-1} (y - F(x)) + (x - a)^T S_a^{-1} (x - a) \quad (2)$$

with respect to **x**. F denotes the physical model relating snowfall parameters to the radar observations and is called the ‘‘forward model”, $\mathbf{S_a}$ is the a priori error covariance matrix and $\mathbf{S_y}$ is the measurement error covariance matrix. $\mathbf{S_y}$ represents not only random instrument noise but also the impact of uncertainties in forward model assumptions on simulated measurements, F(**x**). We use a $\mathbf{S_y}$ standard deviation value of 2 dBZ for this study for the diagonal matrix elements. The optimal-estimation approach weights the magnitude of the error covariances to determine the relative impact of both a priori and observations on the final retrieval estimates. The observation vector, **y**, is the vertical profile of KAZR reflectivities where the retrieval vector, **x**, would be the vertically-varying snowfall particle PSD slope parameter and vertically-uniform number density. The values of **x** that minimize Eq. (2) are found through Newtonian iteration.

Atmos. Meas. Tech. Discuss., doi:10.5194/amt-2017-26, 2017
Manuscript under review for journal Atmos. Meas. Tech.
Discussion started: 15 February 2017

Atmospheric Measurement Techniques Discussions

We introduce MASC PSD information into the retrieval scheme through use of the a priori estimate, **a**, and a priori covariance matrix, $\mathbf{S_a}$. For the PSD slope parameter a priori guess, we processed the MASC images to quantify maximum particle dimension for each snowflake. We then fit a slope parameter for an assumed exponential particle size distribution to the tail of the size distribution > 1 mm in size. We derived estimates of slope parameter either for the entire storm event or for subsections of the event based upon differences in storm morphology. For example, for the April 23 event, we found separate estimates of the slope parameter corresponding to the vertically developed part of the storm before 8 UTC (1.11 mm^{-1}) and for the stratiform part of the storm after 8 UTC (0.74 mm^{-1}). The use of such lengthy time periods was necessary given the infrequent sampling of snowflakes by the MASC at the Barrow site, typically from one to ten snowflakes per minute for these events.

Values for uncertainties in the slope parameter as defined in the a priori error covariance matrix were calculated for the individual storm subsections. These values depended upon both the measure of fit of the exponential slope parameter to MASC observations and expected uncertainties in MASC-derived estimates of particle size from snowflake images. Uncertainties in the slope fit, $\sigma_{\mathbf{FIT}}$, were defined as regression 95% confidence values. Uncertainties in MASC estimates of particle size, $\sigma_{\mathbf{SIZE}}$, were assumed to be 15% of the median maximum particle dimension based upon the preliminary work of Kleinkort et al. (2016). That study used 3-D printed synthetic snowflakes with known geometry to evaluate MASC estimates of particle dimensions using both a 3-camera and 5-camera system. For our study, the variance of the slope parameter guess, $\sigma_{\mathbf{a}}^{\mathbf{2}}$, is then defined as

$$\sigma_a^2 = \sigma_{FIT}^2 + \sigma_{SIZE}^2 . \qquad (3)$$

Table 1 lists estimated slope parameters with uncertainties for the five storm events presented in Section 3. The relatively small uncertainties in the MASC slope parameter observations dictate a solution close to the a priori guess. As a consequence, the uncertainty in the number density must then be left large to allow for retrieval convergence, i.e. allow the particle number to vary so that the forward model simulated reflectivities can match observed radar reflectivities regardless of particle size. The number density term for this scheme is assumed constant with height. Although this approach may be a problem for space-based radars that must see through the entire storm to estimate surface snowfall rate, it is more applicable for use with the upward-looking KAZR. Retrieved snowfall rates are based only the lowest few non-noise radar range bins from 160-300 m above the surface.

Given a retrieved slope parameter and number density, snow water content was estimated for each radar range bin assuming a knowledge of snow particle mass-dimension relationships. As in Figure 4, MASC images are used to select the most appropriate particle model with associated scattering properties for a given scene. The development of more particle models, e.g. lightly rimed aggregates or graupel to better represent the natural variability of observed snowflakes is a current line of

research. In terms of the optimal-estimation technique, this will reduce a major source of uncertainty in the forward model (Sy term in Eq. 2).

Observations of particle fallspeeds from the MASC were used to translate retrieved snow water contents into surface snowfall rates. Figure 5 shows MASC observed snowflake fallspeeds plotted as hourly averages for the April 23 snow event. This plot shows that fallspeeds from the MASC observations were almost always less than those measured from the KAZR Doppler and those predicted from LH74 parameterization schemes (graupel-like snow and aggregates of dendrites). Discrepancies in fallspeed between the MASC and KAZR Doppler observations were expected. Both of these measurements depend upon still air particle fallspeed relationships and atmospheric vertical motion, which is expected to vary between near-surface MASC and aloft Doppler measurements. The MASC observations would also be influenced by near-surface turbulence and disruptions to airflow as the snowflakes pass through the infrared sensors.

The LH74 fallspeeds were estimated through equations 4 and 5 as below,

$V = 1.1\ D^{0.28}$ for Graupel, (4)

$V = 0.8\ D^{0.16}$ for Dendrites, (5)

where the snowflake maximum dimensions used for the LH74 parameterization schemes were calculated using MASC observations. Such discrepancies are in agreement with Garrett and Yuter (2014) who noticed differences between MASC observations of fallspeed at Alta Ski Resort in Utah and LH74 parameterizations. The LH74 schemes predicted fallspeeds poorly for low temperature and highly turbulent environments that might be expected during high-latitude Arctic snow events. Observed fallspeeds are a function of particle- fallspeed relationships and atmospheric vertical motion which may differ throughout the vertical column.

3. Snowfall Retrieval Results

3.1 Snow Events and Retrieval Assumptions

The KAZR- MASC retrieval approach was applied to five snow events as observed at the Barrow site during Spring 2014. KAZR reflectivities for these storms are shown in Figures 4 and 6. These events were selected as they produced measureable snowfall at the nearby Barrow National Weather Service site and triggered co-incident MASC snowflake images. Retrieved estimates of total snowfall accumulation were compared with NWS snowfall observations to evaluate retrieval performance.

Atmos. Meas. Tech. Discuss., doi:10.5194/amt-2017-26, 2017
Manuscript under review for journal Atmos. Meas. Tech.
Discussion started: 15 February 2017

Atmospheric Measurement Techniques Discussions

We examined the impact of snowflake habit, slope parameter (λ), and fallspeed assumptions on retrieved snowfall liquid water equivalent for these events. In terms of habit, we selected the CloudSat B8pr-30 particle model, sector plates, and hexagonal columns. The CloudSat particle model not only performed well in CloudSat snowfall validation studies but also was visually consistent with MASC images of general shape of snowflakes seen at Barrow. Sector plates and hexagonal columns were chosen as they too were observed during these snow events.

For PSD assumptions, we used MASC estimates of slope parameter (λ) with uncertainties as defined through a priori and a priori covariance terms in Equation 2 and Table 1. We also employed an a priori PSD λ assumption (2.8 mm^{-1}) as derived from snowflake observations during the C3VP snow measurement field campaign (Wood et al., 2013) for snow events with similar snowfall rates as the Barrow events. This PSD λ therefore provides a reasonable alternative when lacking co-incident MASC measurements. For fallspeed assumptions, we used MASC and KAZR Doppler observations, LH74 fallspeed parameterizations, and a general 1 m/s value.

We performed retrievals with permutations of habit, PSD, and fallspeed assumptions to determine which combinations produce the best match with snowfall rates observed at the Barrow NWS site. Our best guess or base assumptions were the CloudSat B8pr-30 particle model, MASC fallspeed, and MASC PSD λ. Given the non-unique nature of snowfall retrievals and the difference in location between radar and the NWS office, we do not pretend that agreement between retrieval results and NWS snowfall observations validates our retrieval assumptions. Furthermore, gauge measurements of snowfall amount suffer wind and temperature dependent uncertainties up to at least 25% (Wolff et al., 2014) and cannot be taken at absolute face value. Regardless, these numerical experiments do quantify the sensitivity of snowfall retrieval results to snow microphysical parameters that can be observed by in-situ instrumentation. A better understanding of the impact of these parameters, in turn, should provide a platform in which we can then examine other sources of error in the snowfall problem.

3.2 April 23 Snow Event

Radar reflectivities and MASC images for an April 23 snow event that produced a total snow accumulation 0.18 inches liquid equivalent are shown in Figure 4. Retrieval results assuming different particle model, slope parameter, and fallspeed combinations as described in section 3.1 are presented in Table 2. The percentage difference term in the table is defined through Eq. (6),

Atmos. Meas. Tech. Discuss., doi:10.5194/amt-2017-26, 2017
Manuscript under review for journal Atmos. Meas. Tech.
Discussion started: 15 February 2017

Atmospheric Measurement Techniques Discussions

$$\%\ Difference = \frac{(Retrieved\ Snowfall - NWS\ Snowfall)}{NWS\ Snowfall} * 100. \quad (6)$$

Error values ranged from -51% to +132% for this snow event. We found the best agreement with the NWS observations using our 'base' assumptions of MASC fallspeed and PSD λ, CloudSat B8pr-30 particle model with a retrieved accumulated snowfall of 0.192 inches liquid equivalent, a difference of +7%. This accuracy was closely matched with use of the combination of hexagonal columns, KAZR Doppler fallspeeds, and the PSD λ from the MASC. For these two scenarios, the highly reflective per unit mass hexagonal columns and high fallspeed Doppler observations offset the lower reflective per unit mass CloudSat particle model and low fallspeed MASC observations to produce nearly equivalent snow accumulations. Since hexagonal columns were not observed during the snowstorm, however, that solution is not valid. Worst agreement (+132%) arose from use of the MASC PSD λ, the CloudSat B8pr-30 particle model, and the LH74 graupel fallspeed. This large discrepancy was driven by the high fallspeed of the LH74 graupel parameterization as seen in Figure 5.

These calculations allowed us to quantify the sensitivity of retrieval results to assumptions of PSD λ, fallspeed, and crystal habit for a given storm event. Assumed PSD slope parameter had the least impact on variability in estimated snowfall accumulation. Snowfall totals of 0.19 inches and 0.24 inches were found when using the MASC PSD λ and the C3VP field campaign observed PSD λ, respectively, holding fallspeed and habit fixed. In terms of the optimal-estimation scheme, changes in the PSD λ are offset by corresponding changes in the PSD number density. So, larger particles (smaller slope parameter) require fewer particles to match radar reflectivity, and vice versa. Such a relationship modulates the impact of changes in particle size distribution on estimated snowfall rates.

By contrast, differing assumptions of fallspeed led to a factor of 2 differences in retrieved snowfall rates. Accumulations varied from 0.19 inches with MASC fallspeed observations to 0.42 inches with LH74 graupel-like snow parameterizations, holding base habit and PSD fixed. These results were driven by the variability in fallspeeds as plotted in Figure 5 and the linear impact of fallspeed on retrieved snowfall rate. Interestingly, retrieved snowfall rates using low level Doppler fallspeeds were twice those found using MASC fallspeed observations. Such results imply the need for further research to determine which or either fallspeed observation is appropriate for a given scene.

Differing assumptions of particle model also led to a factor of 2 differences in retrieved snowfall rates. Estimated snowfall accumulations varied from 0.19 inches for the CloudSat B8pr-30 particle model to 0.09 inches for hexagonal columns, given fixed fallspeed and PSD assumptions. NWS 'truth' (0.18 inches) fell between results assuming the branched CloudSat particle (0.19 inches) and sectored plates (0.13 inches) where both of these habits were seen during the storm event as in

Atmos. Meas. Tech. Discuss., doi:10.5194/amt-2017-26, 2017
Manuscript under review for journal Atmos. Meas. Tech.
Discussion started: 15 February 2017

Atmospheric Measurement Techniques Discussions

Figure 4. Given the presence of rimed particles throughout the storm, however, we would not expect perfect agreement given use of non-rimed particle models for the retrieval.

3.3 May 15 Snow Event

Table 3 lists retrieved accumulated snowfall amounts for a May 15 snow event as depicted in the upper left panel of Figure 6. This storm produced approximately 0.30 inches liquid equivalent of snowfall as observed by the NWS before transitioning to light rainfall. Although the use of our base CloudSat particle model, MASC fallspeed, and MASC λ assumptions produced snowfall estimates close to NWS observations for the April 23 event, these same assumptions performed poorly for this storm. We found a -43% difference relative to NWS observations.

For all retrieval permutations, differences between retrieved snowfall and NWS observations varied from -74% to +56%. The best agreement to NWS values came with the permutation of sector plates, MASC λ, and KAZR Doppler fallspeed assumptions (+6%). The next best agreement came with the use of CloudSat B8pr-30 particle model, MASC λ, and LH74 dendritic aggregate fallspeed assumptions (-10%). Again, it is the compensating nature of fallspeed and particle model for these two different retrieval permutations that allow them to produce results consistent with NWS observations. Agreement was particularly poor for those cases that assumed the highly reflective hexagonal column particle model, e.g. a difference of -74% was found with columns when used with MASC observed fallspeeds and PSD λ. The use of highly reflective columns (which were not seen during the event) could not generate enough retrieved snowfall to match observations regardless of fallspeed assumptions.

A possible reason for these observed discrepancies in this case is the presence of heavy riming in observed snowflakes. MASC images suggest lumpy graupel-like snowflakes and aggregates throughout the entire snow event as shown in Figure 7. Such particles would be expected to be denser and thus have more mass for given maximum dimension than the un-rimed particle models employed in this study. Such conditions would cause the snowfall retrievals to underestimate snow rate, all other variables fixed. Similarly, particle- backscatter relationship would change given a coating of frozen or possibly liquid water on the particles, further biasing results. These topics, such as rimed particle scattering calculations and development of a hot plate to measure mass-dimension relationships, are the focus of future work.

3.4 Totals for Five Snow Events

Table 4 lists total retrieved liquid water equivalent over the five snow events at Barrow for different retrieval assumption permutations. The approximate accumulated snowfall was 0.63 inches liquid equivalent for these five events as measured by

Atmos. Meas. Tech. Discuss., doi:10.5194/amt-2017-26, 2017
Manuscript under review for journal Atmos. Meas. Tech.
Discussion started: 15 February 2017

Atmospheric Measurement Techniques Discussions

the nearby NWS site. Use of our base assumptions (MASC fallspeed, MASC PSD λ, and CloudSat particle model) led to total accumulated snowfall of 0.52 inches, which represents a difference of -18% relative to NWS observations.

Use of the C3VP a priori PSD λ led to a slightly better match with NWS observations (-3%) than use of MASC PSD λ (-18%) when used with base particle model and fallspeed assumptions. These results are not surprising given that the a priori λ value of 2.8 mm^{-1} falls within the range of observed MASC PSD λ values from 0.74 to 3.42 mm^{-1}. The average error for the individual snow events, however, was similar for the two λ assumptions. Value of 43% and 44% were found for C3VP and MASC PSD, respectively.

Other assumption permutations found retrieved liquid water accumulations with differences ranging from -64% to + 94% relative to NWS observations. These results again highlight the likelihood of compensating errors when inverting radar observations to estimate snowfall. Best agreement (3%) came for two retrieval scenarios with different assumptions for each habit, PSD λ, and fallspeed. The CloudSat particle model, C3VP a priori PSD λ, and MASC fallspeed combination resulted in 3% less retrieved snowfall than NWS observations. Sector plates, MASC PSD λ, and a 1 m/s fallspeed resulted in 3% more retrieved snowfall than NWS observations. To further illustrate this idea of compensating uncertainties, consider the use of assumptions that are all demonstrably wrong (hexagonal columns, 1 m/s fallspeed, and C3VP a priori PSD λ) for the vast majority of these observed snow events. This retrieval permutation generates a value for accumulated snowfall of 0.47 inches that is very close to the 0.52 inches found using our base assumptions. In the next section, we will discuss implications of these results for the utility of ground-based in-situ measurements to refine and improve estimates of snowfall from radar measurements.

4 Discussion and Conclusions

In this work, we present an optimal-estimation retrieval scheme to calculate surface snowfall rates using coincident radar and in-situ snow particle observations. The scheme was modified from the W-band CloudSat snowfall algorithm and applied to measurements from the ground-based Ka-band Zenith Radar (KAZR) located at the ARM NSA Barrow Climate Facility Site. Multi-Angle Snow Camera (MASC) estimates of particle size distribution and fallspeed were used to constrain the inverse calculations based upon KAZR reflectivities. Images of snowflakes from the MASC were used as a guide to select the most appropriate particle model for a given storm event, e.g. branched aggregates, sector plates, or columns. Retrieved snowfall accumulation were compared with snowfall measurements at the nearby NWS Barrow office for a first order evaluation of our results.

Atmos. Meas. Tech. Discuss., doi:10.5194/amt-2017-26, 2017
Manuscript under review for journal Atmos. Meas. Tech.
Discussion started: 15 February 2017

Atmospheric Measurement Techniques Discussions

Retrieval snowfall values found using MASC observations as assumptions were contrasted with those found using alternate assumptions such as Locatelli and Hobbs fallspeed parameterizations, Doppler fallspeed observations, and field campaign observations of snow particle size distributions. Use of these different permutations of retrieval assumptions (habit, PSD λ, and fallspeed) allowed us to determine which combination of assumptions best matched nearby NWS snowfall observations for five different snow events. Differences between these approaches also quantified the sensitivity of estimated snowfall amounts to PSD λ, particle fallspeed, and snowflake particle model. Although the number of events and snowfall totals with co-incident MASC and KAZR observations is limited, they do provide an initial data set to quantify retrieval performance across multiple snow events.

Use of the base assumptions (CloudSat particle model, MASC fallspeed, and MASC PSD λ) resulted in estimated snowfall totals over the five events with a -18% difference relative to nearby NWS snowfall observations. The average absolute difference was 45% for the individual events. These results suggest that modification of the CloudSat particle model to Ka-band frequency and use of MASC observations can produce reasonable snowfall values for spring conditions at Barrow. This agrees in spirit with the validation studies from the C3VP Program in which simulated reflectivities using the CloudSat particle model matched well with field observations as demonstrated in Figure 2.

Other combinations of retrieval assumptions found differences in accumulated snowfall ranging from -64% to +94% relative to NWS observations as listed in Table 4. However, the non-unique nature of the snowfall retrieval problem makes it difficult to determine if we get good results for the 'right reasons'. For example, the use of a trio of assumptions (hexagonal column particle model, C3VP a priori PSD λ, and a 1 m/s fallspeed) that are all demonstrably wrong yields overall differences (-25%) that are similar to those found with our base assumptions (-18%). For this 'wrong' scenario, compensating errors in fallspeed (bias results high) and particle model (bias results low) offset to produce snowfall results that are reasonable. Furthermore, perfect agreement between retrieval results and NWS snowfall observations cannot provide complete validation of our assumptions. Wolff et al. (2014) found that snowfall gauge measurements can suffer significant uncertainties that are a complex function of atmospheric environment, so they cannot be taken as absolute truth for validation especially given the limited snowfall totals for these spring Barrow events.

Use of alternate fallspeed and particle model assumptions led to factor of 2 differences in retrieved snowfall rates when averaged over the five snow events. Assumed PSD slope parameter had less impact on variability in estimated snowfall accumulation. Snowfall totals of 0.52 inches and 0.61 inches were found when using the MASC PSD λ and the C3VP field campaign observed PSD λ, respectively, holding fallspeed and habit fixed. In terms of the optimal-estimation approach, changes in the PSD λ are offset by corresponding changes in the particle number density. Larger particles require fewer

particles to match radar reflectivity, and vice versa, thus limiting the impact on estimated snow water content with changing particle size.

Significant sensitivities to multiple variables imply difficulties for the evaluation and design of snowfall retrieval schemes. Those studies that focus on one or even a few variables may vary likely lead to misleading conclusions. Meaningful advancements in the retrieval problem will require a comprehensive approach that considers coincident in-situ observations of habit, PSD, fallspeed and other variables such as particle orientation. Incremental improvements in the understanding of any of these parameters dependent upon specific location and meteorological conditions will help reduce retrieval non-uniqueness and should allow insights into the other sources of error for the approach.

Future work will continue to explore the coincident radar and ground-based in-situ instrumentation approach presented here. We will modify existing particle models and DDA scattering properties based upon information from the MASC images. For example, MASC images shown in Figures 4 and 7 suggest some degree of riming for most snowflakes even for the cold Barrow site. Differences in the scattering properties and mass-dimensional relationships for rimed and un-rimed particles are anticipated to explain the large discrepancies in retrieved and observed snowfall rates observed for the rimed May 15 case. Likewise, we will seek to determine the most appropriate fallspeed metric given available instrumentation. Large discrepancies were observed between near-surface MASC fallspeed measurements, lowest radar range bin Doppler velocities, and particle fallspeed-dimension parameterizations. Such studies also will require the quantification of sampling artifacts for the MASC or other in-situ microphysical instrumentation through efforts similar to Kleinkort et al. (2016).

Given the limited data available from the NSA Barrow site, we stress the need for more data sets with coincident radar, snowfall microphysical, and snow gauge observations. The general technique presented here for the KAZR and MASC could be adapted to any set of coincident radar and PSD instrumentation. Along these lines, the authors are deploying a Micro Rain Radar, MASC, and Precipitation Imaging Package (PIP) to two state-of-the-art snowfall measurements field sites in Scandinavia over the next couple of winters. These sites, one run by the Norwegian Meteorological Institute near Haukeliseter and one by the Swedish Meteorological and Hydrological Institute near Åre, experience numerous snowfall events representing a diverse range of synoptic and mesoscale conditions. Such a comprehensive set of observations should allow us to refine our retrieval approach and to gain insights into the state-dependence of snowfall microphysics. In turn, these improved snowfall estimates could be used to explain observed differences in ground and satellite-based radar estimates of snowfall (Cao et al., 2014; Smalley et al. 2014; Norin et al., 2015) or as input for weather and climate studies.

Acknowledgments

Data were obtained from the Atmospheric Radiation Measurement (ARM) Program sponsored by the U.S. Department of Energy, Office of Science, Office of Biological and Environmental Research, Climate and Environmental Sciences Division.

All authors were supported through National Science Foundation grant 1531930 and Department of Energy grant DE-SC0016045. In addition, parts of this research conducted by N. Wood and T. L'Ecuyer were performed at the University of Wisconsin- Madison for the Jet Propulsion Laboratory, California Institute of Technology, sponsored by National Aeronautics and Space Administration CloudSat Research Grant G-3969-1. Parts of the original code development by S. Cooper was performed under NASA grant number NNX15AK17G and NSF grant 1303965. We thank Tim Garrett for processing the MASC data to estimate particle size.

References

Brown, R. D., 2000: Northern Hemisphere snow cover variability and change, 1915–1997. *J. Climate*, **13**, 2339–2355.

Brown, R., C. Derksen, and L. Wang (2010), A multi-data set analysis of variability and change in Arctic spring snow cover extent, 1967–2008, *J. Geophys. Res.*, *115*, D16111, doi:10.1029/2010JD013975.

Cao, Q., Hong, Y., Chen, S., Gourley, J. J., Zhang, J., and Kirstetter, P. E.: Snowfall detectability of NASA's CloudSat: the first cross-investigation of its 2c-snow-profile product and national multi-sensor mosaic QPE (NMQ) snowfall data, Prog. Electromagn.Res., 148, 55–61, doi:10.2528/PIER14030405, 2014.

Christensen, M. W., A. Behrangi, T. L'Ecuyer, N. B. Wood, M. D. Lebsock, and G. L. Stephens, 2016: Arctic Observation and Reanalysis Integrated System: A new data product for validation and climate study. Bull. Am. Meteor. Soc., doi:10.1175/BAMS-D-14-00273.1, in press.

Cohen, J., and D. Rind, 1991: The effect of snow cover on the climate. J. Clim., **4**, 689-706.

Draine, B. T., and P. J. Flatau, 1994: Discrete-dipole approximation for scattering calculations. J. Opt. Soc. Amer., 11A, 1491-1499.

Dyurgerov, M., and M. F. Meier, 2005: Glaciers and changing Earth system: a 2004 snapshot, INSTAAR, Boulder.

Frauenfeld, O. W., T. Zhang, R. G. Barry, and D. Gilichinsky (2004), Interdecadal changes in seasonal freeze and thaw depths in Russia, *J. Geophys. Res.*, **109**, D05101, doi:10.1029/2003JD004245.

Gardner A. S. et al.: A Reconciled Estimate of Glacier Contributions to Sea Level Rise: 2003 to 2009, *Science* 17 May 2013: Vol. 340, Issue 6134, pp. 852-857. DOI: 10.1126/science.1234532

Garrett, T. J., Fallgatter, C., Shkurko, K., and Howlett, D.: Fallspeed measurement and high-resolution multi-angle photography of hydrometeors in freefall, Atmos. Meas. Tech. Discuss., 5, 4827-4850, doi:10.5194/amtd-5-4827-2012, 2012.

Garrett, T. J., and S. E. Yuter (2014), Observed influence of riming, temperature, and turbulence on the fallspeed of solid precipitation, Geophys. Res. Lett., 41, 6515–6522, doi:10.1002/2014GL061016.

Heymsfield, A. J., P. Field, and A. Bansemer, 2008: Exponential size distributions for snow. *J. Atmos. Sci.*, **65**, 4017–4031, doi:10.1175/2008JAS2583.1.

Holland, M.M, and C.M. Bitz (2003), Polar amplification of climate change in coupled models, *Clim. Dyn.*, **21**, 221–232.

Holland, M.M., C.M. Bitz, and L.-B. Tremblay (2006), Future abrupt reductions in the summer arctic sea ice. *Geophys Res. Lett.,* **33**, L23503, doi:10.1029/2006GL028024.

Hudak, D. R., H. W. Barker, P. Rodriguez, and D. P. Donovan (2006), The Canadian CloudSat Validation Project, paper presented at 4th European Conference on Radar in Hydrology and Meteorology, Servei Meteorolog. de Catalunya (Meteocat), Barcelona, Spain, 18 – 22 Sept.

Jacob, T., J. Wahr, W.T. Pfeffer, and S. Swenson, 2012: Recent contributions of glaciers and ice caps to sea level rise. *Nature*, **482**, 514–518, DOI: 10.1038/nature10847.

Kleinkort, C., G.-J. Huang, V. N. Bringi, and B.M. Natoro: 2016: Visual Hull Method for Realistic 3D Particle Shape Reconstruction Based on High-Resolution Photographs of Snowflakes in Freefall from Multiple Views, J. Atmos. Oceanic Technol., DOI: http://dx.doi.org/10.1175/JTECH-D-16-0099.1.

Kulie, M.S. and R. Bennartz, Utilizing spaceborne radars to retrieve dry snowfall, J. Applied Meteor. and Climat., **48**, Issue 12, 2564-2580.

Kulie, M. S., L. Milani, N. B. Wood, S. A. Tushaus, and T. S. L'Ecuyer, 2016: A shallow snowfall census using spaceborne radar. J. Hydromet., accepted.

Liu, G. (2008), Deriving snow cloud characteristics from CloudSat observations, *JGR*, VOL. 113, D00A09, 13 PP., 2008 doi:10.1029/2007JD009766

Lenaerts, J. T. M., J. H. van Angelen, M. R. van den Broeke, A. S. Gardner, B. Wouters and E. van Meijgaard (2013), Irreversible mass loss of Canadian Arctic Archipelago glaciers, Geophys. Res. Lett., 40, 870–874, doi:10.1002/grl.50214.

Locatelli, J. D., and P. V. Hobbs (1974), Fall speeds and masses of solid precipitation particles, J. Geophys. Res., 79(15), 2185–2197, doi:10.1029/JC079i015p02185.

Manabe, S., and R. J. Stouffer (1980), Sensitivity of a Global Climate Model to an Increase of CO2 Concentration in the Atmosphere, J. Geophys. Res., 85(C10), 5529–5554, doi:10.1029/JC085iC10p05529.

Matrosov, S.Y., M.D. Shupe, and I.V. Djalalova (2007), Snowfall Retrievals Using Millimeter-Wavelength Cloud Radars, *JAMC*, **47,** 769-777. DOI: 10.1175/2007JAMC1768.1

Newman, A. J., Kucera, P. A., and Bliven, L. F.: Presenting the snowflake video imager (SVI), J. Atmos. Ocean. Tech., 26, 167–179, 2009.

Noh, Y.-J., G. Liu, E.-K. Seo, J. R. Wang, and K. Aonashi (2006), Development of a snowfall retrieval algorithm at high microwave frequencies, J. Geophys. Res., 111, D22216, doi:10.1029/2005JD006826.

Norin, L., Devasthale, A., L'Ecuyer, T. S., Wood, N. B., and Smalley, M.: Intercomparison of snowfall estimates derived from the CloudSat Cloud Profiling Radar and the ground-based weather radar network over Sweden, Atmos. Meas. Tech., 8, 5009-5021, doi:10.5194/amt-8-5009-2015, 2015.

Palerme, C., J. E. Kay, C. Genthon, T. L'Ecuyer, N. B. Wood, and C. Claud, 2014: How much snow falls on the Antarctic ice sheet? *The Cryosphere*, **8**, 1577-1587.

Palerme, C., C. Genthon, C. Claud, J. E. Kay, N. B. Wood, T. L'Ecuyer, 2016: Evaluation of current and projected Antarctic precipitation in CMIP5 models, Clim. Dyn., accepted.

Perlwitz J., M. Hoerling, and R. Dole, 2015: Arctic Tropospheric Warming: Causes and Linkages to Lower Latitudes. *J. Climate*, **28**, 2154–2167. doi: http://dx.doi.org/10.1175/JCLI-D-14-00095.1

Peterson, B. J., J. McClelland, R. Curry, R. M. Holmes, J. E. Walsh, and K. Aagaard, 2006: Trajectory shifts in the Arctic and subarctc freshwater cycle. Science, **313**, doi:10.1126/science.1122593.

Rodgers, C.D., 2000: Inverse Methods for Atmospheric Sounding. World Scientific Publishing, 256 pp.

Romanovsky, V., M. Burgess, S. Smith, K. Yoshikawa, and J. Brown, 2002: Permafrost Temperature Records: Indicators of Climate Change. *EOS, AGU Transactions*, **83**(50), 589–594.

Serreze, M. C., J. E. Walsh, F. S. Chapin, T. Osterkamp, M. Dyurgerov, V. Romanovsky, W. C. Oechel, J. Morison, T. Zhang, and R. Barry, 2000: Observational evidence of recent change in the northern high-latitude environment. *Climatic Change*, **46**, 159–207.

Serreze, M.C., and J. A. Francis (2006), The Arctic amplification debate, *Climatic Change*, **76**, 241–264.

Skofronick-Jackson, G. M., M. J. Kim, J. A. Weinman, D. E. Chang (2004), A physical model to determine snowfall over land by microwave radiometry, *IEEE Trans. Geosci. Remote Sens*., *42*, 1047-1058.

Smalley, M., L'Ecuyer, T., Lebsock, M., and Haynes, J.: A comparison of precipitation occurrence from the NCEP StageIV QPE Product and the CloudSat Cloud Profiling Radar, J. Hydrol., 15,444–458, doi:10.1175/JHM-D-13-048.1, 2014.

Stroeve, J., M. Serreze, S. Drobot, S. Gearheard, M. Holland, J. Maslanik, W. Meier, and T. Scambos (2008), Arctic sea ice extent plummets in 2007, *EOS, Trans. Am. Geophys. Union*, **89**, 13–14.

Stroeve, J. C., T. Markus, L. Boisvert, J. Miller, and A. Barrett (2014), Changes in Arctic melt season and implications for sea ice loss, Geophys. Res. Lett., 41, 1216–1225, doi:10.1002/2013GL058951.

Van Tricht, K., S. Lhermitte, J. T. M Lenaerts, I. V. Gorodetskaya, T. L'Ecuyer, B. Noel, M. R. van den Broeke, D. D. Turner, and N. P. M. van Lipzig, 2016: Clouds enhance Greenland ice sheet meltwater runoff *Nature Communications*, **7**.

Vavrus, S., 2007: The role of terrestrial snow cover in the climate system. Clim. Dyn., **29**, doi:10.1007/s00382-007-0226-0, 73-88.

Wolff, M. A., Isaksen, K., Petersen-Øverleir, A., Ødemark, K., Reitan, T., and Brækkan, R.: Derivation of a new continuous adjustment function for correcting wind-induced loss of solid precipitation: results of a Norwegian field study, Hydrol. Earth Syst. Sci. Discuss., 11, 10043-10084, doi:10.5194/hessd-11-10043-2014, 2014.

Wood, N. B., 2011: Estimation of snow microphysical properties with application to millimeter-wavelength radar retrievals for snowfall rate. Ph. D. dissertation, Colorado State University, 231 pp.

Wood, N. B., and T. S. L'Ecuyer, 2013: Level 2C Snow Profile Product Process Description and Interface Control Document, NASA Jet Propulsion Laboratory, available from http://www.cloudsat.cira.colostate.edu/ICD/2C-SNOW-PROFILE/2C-SNOW-PROFILE_PDICD_P_R04.pdf

Wood, N. B., T. S. L'Ecuyer, A. J. Heymsfield, G. L. Stephens, D. R. Hudak, and P. Rodriguez (2014), Estimating snow microphysical properties using collocated multisensor observations, J. Geophys. Res. Atmos., 119, 8941–8961 doi:10.1002/2013JD021303.

Wood, N.B., Tristan S. L'Ecuyer, Andrew J. Heymsfield, and Graeme L. Stephens, 2015: Microphysical Constraints on Millimeter-Wavelength Scattering Properties of Snow Particles. *J. Appl. Meteor. Climatol.*, **54**, 909–931. doi: http://dx.doi.org/10.1175/JAMC-D-14-0137.1

Atmos. Meas. Tech. Discuss., doi:10.5194/amt-2017-26, 2017
Manuscript under review for journal Atmos. Meas. Tech.
Discussion started: 15 February 2017

Atmospheric Measurement Techniques Discussions

Table 1: MASC observed slope parameters for exponential particle size distributions for the Barrow snow events. The C3VP observations were derived from field observations with similar snow rates as the Barrow storms (Wood et al., 2013).

Event	PSD Slope Parameter, λ	Uncertainty in λ
April 23 00-08 UTC	1.11	± 0.23
April 23 08-24 UTC	0.74	± 0.15
May 15 04-23 UTC	1.08	± 0.25
May 17 11-18 UTC	1.44	± 0.29
May 17 18-24 UTC	0.74	± 0.51
May 21 20-24 UTC	3.42	± 0.64
May 26 08-17 UTC	2.09	± 0.68
C3VP Field Observations	2.8	± 0.5

Table 2: Retrieved snowfall amounts for an April 23 snow event for designated retrieval assumption combinations. Nearby NWS observations suggested 0.18 inches of snowfall liquid equivalent. The MASC-derived PSD slope parameters (λ) used for this event are listed in Table 1.

Particle Model	λ (PSD slope)	Fallspeed	Snowfall (in)	% Difference
CloudSat	MASC	MASC obs	0.192	+7
CloudSat	MASC	Doppler	0.361	+100
CloudSat	MASC	LH74, Aggs Den	0.285	+58
CloudSat	MASC	LH74, Graupel	0.418	+132
CloudSat	MASC	1 m/s	0.327	+82
CloudSat	Field- C3VP	MASC obs	0.239	+33
Sector Plates	MASC	MASC obs	0.131	-27
Sector Plates	MASC	Doppler	0.248	+38
Sector Plates	MASC	1 m/s	0.225	+25
Sector Plates	Field- C3VP	1 m/s	0.237	+32
Hex Columns	MASC	MASC obs	0.088	-51
Hex Columns	MASC	Doppler	0.167	-7

Atmos. Meas. Tech. Discuss., doi:10.5194/amt-2017-26, 2017
Manuscript under review for journal Atmos. Meas. Tech.
Discussion started: 15 February 2017

Atmospheric Measurement Techniques Discussions

Table 3: Retrieved snowfall amounts for a May 15 snow event for retrieval assumption combinations. Nearby NWS observations suggested 0.30 inches of snowfall liquid equivalent. The MASC-derived PSD slope parameters (λ) used for this event are listed in Table 1.

Particle Model	λ (mm^-1)	Fallspeed	Snowfall (in)	% Difference
CloudSat	MASC	MASC obs	0.171	- 43
CloudSat	MASC	Doppler	0.469	+ 56
CloudSat	MASC	LH74, Aggs Den	0.271	- 10
CloudSat	MASC	LH74, Graupel	0.379	+ 26
CloudSat	MASC	1 m/s	0.331	+ 10
CloudSat	Field- C3VP	MASC obs	0.210	- 30
Sector Plates	MASC	MASC obs	0.116	- 61
Sector Plates	MASC	Doppler	0.319	+ 6
Sector Plates	MASC	1 m/s	0.225	- 25
Sector Plates	Field- C3VP	1 m/s	0.237	- 21
Hex Columns	MASC	MASC obs	0.078	- 74
Hex Columns	MASC	Doppler	0.216	- 28

5

Table 4: Total retrieved snowfall amounts over five Barrow snow events for designated retrieval assumption combinations. Nearby NWS observations suggested 0.63 inches of snowfall liquid equivalent. The MASC-derived PSD slope parameters (λ) used for these events are listed in Table 1.

Particle Model	λ (mm^-1)	Fallspeed	Snowfall (in)	% Difference
CloudSat	MASC	MASC obs	0.516	-18
CloudSat	MASC	Doppler	1.195	+90
CloudSat	MASC	LH74, Aggs Den	0.811	+29
CloudSat	MASC	LH74, Graupel	1.22	+94
CloudSat	MASC	1 m/s	1.009	+60
CloudSat	Field- C3VP	MASC obs	0.609	-3
Sector Plates	MASC	MASC obs	0.338	-46
Sector Plates	MASC	Doppler	0.777	+23
Sector Plates	MASC	1 m/s	0.648	+3
Sector Plates	Field- C3VP	1 m/s	0.677	+7
Hex Columns	MASC	MASC obs	0.228	-64
Hex Columns	MASC	Doppler	0.527	-16
Hex Columns	Field- C3VP	1m/s	0.470	-25

Atmos. Meas. Tech. Discuss., doi:10.5194/amt-2017-26, 2017
Manuscript under review for journal Atmos. Meas. Tech.
Discussion started: 15 February 2017

Atmospheric Measurement Techniques Discussions

Figures

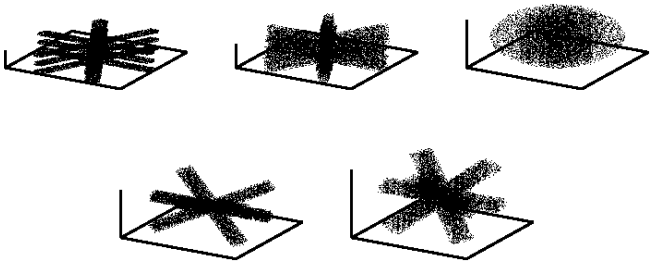

Figure 1: Discrete dipole models, clockwise from upper left: Sector plate, SPp; 6-branched planar rosette, B6pf; ellipsoid, Ep; 8-branched rosette with 0.5 aspect ratio, B8pr-30; 8-branched rosette with 0.7 aspect ratio, B8pr-45 as taken from Wood et al. (2015).

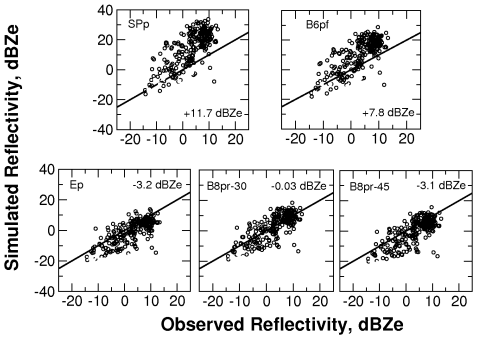

Figure 2: Comparisons of observed W-band reflectivities with synthetic reflectivities derived from the DDA scattering properties as taken from a modified figure from Wood et al. (2015).

Atmos. Meas. Tech. Discuss., doi:10.5194/amt-2017-26, 2017
Manuscript under review for journal Atmos. Meas. Tech.
Discussion started: 15 February 2017

Atmospheric Measurement Techniques Discussions

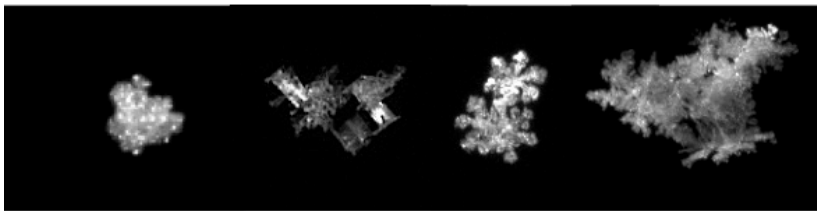

Figure 3. MASC-captured images of snowflakes as observed at the NSA Barrow Climate Facility site.

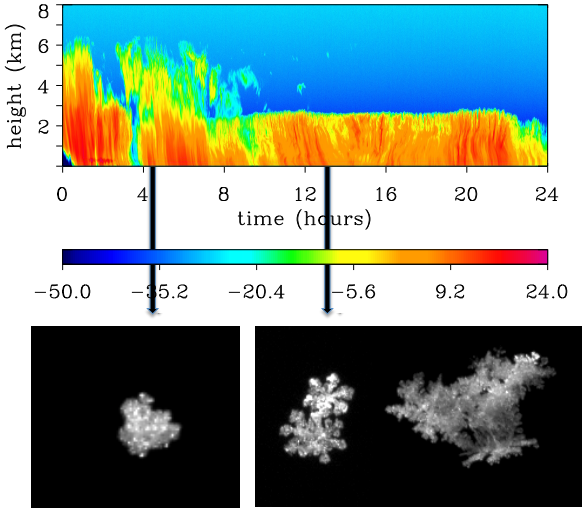

Figure 4: The top scene shows KAZR reflectivities (dBZ) for an April 23 snow event at the NSA Barrow site. MASC images of snowflakes suggest a graupel-like structure around 4 UTC which transitioned to more pristine structures and aggregates by 13 UTC.

Atmos. Meas. Tech. Discuss., doi:10.5194/amt-2017-26, 2017
Manuscript under review for journal Atmos. Meas. Tech.
Discussion started: 15 February 2017

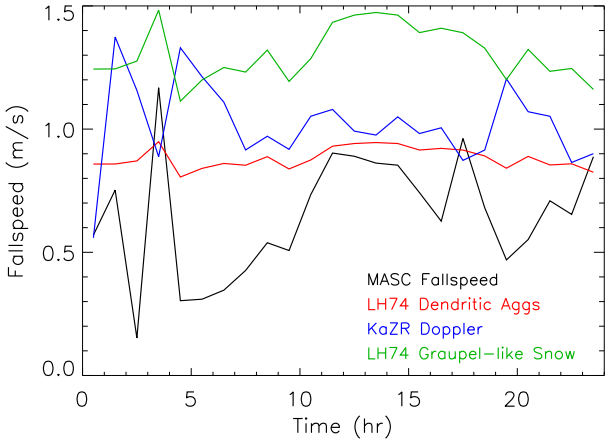

Figure 5. MASC observed fallspeeds for April 23 snowfall event at Barrow are plotted in black. Results are compared to calculations from LH74 parameterization schemes for crystal types similar to those observed by MASC during the storm event. Green represents graupel-like snow while red represents dendritic aggregates. Near surface Doppler fallspeeds from the KAZR are plotted in blue.

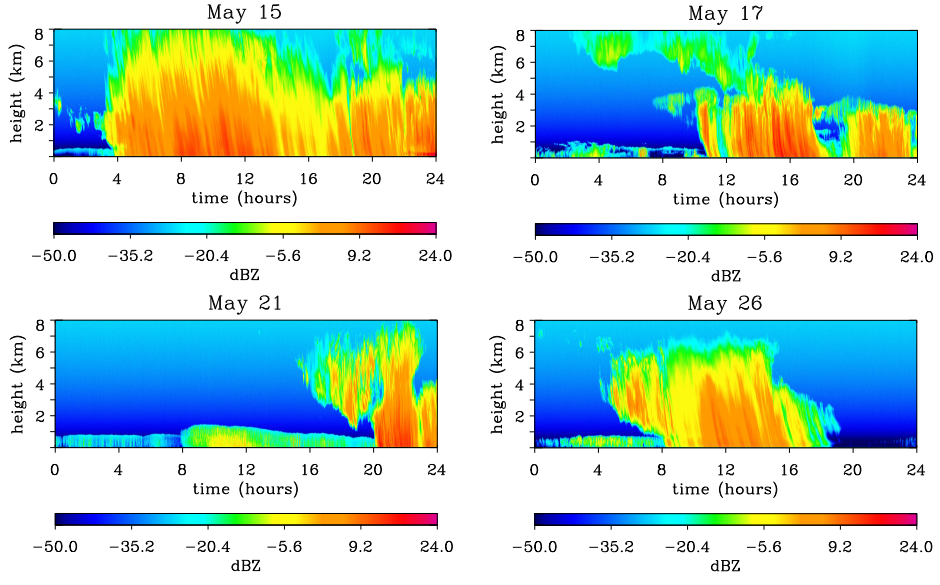

Figure 6: KAZR reflectivities (dBZ) for snow event systems as observed at the NSA Barrow Climate Facility site.

Atmos. Meas. Tech. Discuss., doi:10.5194/amt-2017-26, 2017
Manuscript under review for journal Atmos. Meas. Tech.
Discussion started: 15 February 2017

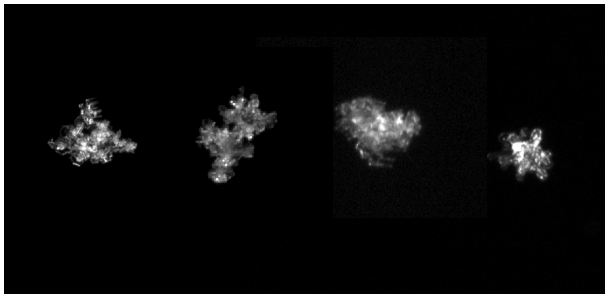

Figure 7: Typical rimed and graupel-like particles observed by the MASC on May 15.